Inorganic Chemistry
Article

Inorg. Chem. **2011**, *50*, 365–377 **365**
DOI: 10.1021/ic102151p

Ditopic Complexation of Selenite Anions or Calcium Cations by Pirenoxine: An Implication for Anti-Cataractogenesis

Jiahn-Haur Liao,[†,○] Chien-Sheng Chen,[†,○] Chao-Chien Hu,[‡,§,∥] Wei-Ting Chen,[⊥] Shao-Pin Wang,[⊥] I-Lin Lin,[#] Yi-Han Huang,[†] Ming-Hsuan Tsai,[#] Tzu-Hua Wu,[*,#] Fu-Yung Huang,[*,⊥] and Shih-Hsiung Wu[*,†]

[†]*Institute of Biological Chemistry, Academia Sinica, Taipei 115, Taiwan,* [‡]*Department of Ophthalmology, Shin Kong Wu Ho-Su Memorial Hospital, Taipei 111, Taiwan,* [§]*School of Medicine, Fu-Jen Catholic University, Hsinchuang, 242, Taiwan,* [∥]*School of Medicine, Taipei Medical University, Taipei 110, Taiwan,* [⊥]*Department of Chemistry, National Cheng Kung University, Tainan 701, Taiwan, and* [#]*School of Pharmacy, College of Pharmacy, Taipei Medical University, Taipei 110, Taiwan.* [○] *Equal contribution to this work.*

Received October 26, 2010

This study investigated whether and how pirenoxine (PRX) interacts with selenite or calcium ions, as these two ions have been proven respectively a factor leading to the formation of lens cataract. UV, NMR, and isothermal titration calorimetry (ITC) analysis indicated that PRX could bind maximum up to six selenite anions and the binding site preference was concentration dependent with the peripheral binding first followed by the $\pi-\pi$ interactions with the aromatic moiety; while for calcium cation interaction the 3-carboxylate and β-ketoimine functional groups were responsible for chelating calcium ions. The results obtained by MP2/6-31+G(d) molecular orbital calculations provided theoretical evidence in support of the $\pi-\pi$ interactions between selenite and the PRX aromatic framework, and further analysis of the binding energies with the aromatic moiety indicates that these interactions take place most likely at the benzoquinone (ring I) π-system. The calcium binding preferences with PRX were also determined based on the stabilization energy obtained by B3LYP/6-31+G(d) calculations, showing the binding preferences were site 2 > site 1 > site 3 > ring II, consistent with the experimental data. The in vitro study of the reduction of selenite or calcium ions-induced lens turbidity by PRX with ditopic recognition properties was thus demonstrated. These results may provide a rationale for using PRX as an anti-cataract agent and warrant further biological studies.

1. Introduction

Excessive calcium ions can be detrimental to cells, and raised levels of calcium ions in human lenses with cortical cataracts have been found to play important roles in the opacification process.[1,2] Incubating human lenses in media containing high levels of Ca^{2+} has been shown to result in a loss of transparency in the cortex of the lens.[3] The increase of calcium ions in lenses was then correlated to the proteolysis of lens crystallins.[4−6] Lens turbidity[7] is thought to occur either because of the activation of calpain, a protease present in the lens, or simply because of lens crystallin aggregation.[8] Crystallin loss increases with time as lens calcium continues to increase, and the Ca^{2+}-activated protease, calpain, is thought to be responsible for the proteolysis of lens crystallins.[4,9,10]

Aside from calcium, selenite has also shown the effects of causing cataracts in an animal model study as reported earlier in 1977.[11,12] Our previous study also found that selenite ions could cause lens protein precipitation.[13] Accumulation of Se in the soluble and insoluble proteins of the lens[14] and the development of cortical opacities in selenite-containing medium[15]

*To whom correspondence should be addressed. E-mail: thwu@tmu.edu.tw (T.-H. Wu), fhuang@mail.ncku.edu.tw (F.-H. Huang), shwu@gate.sinica.edu.tw (S.-H. Wu).

(1) Rhodes, J. D.; Sanderson, J. *Exp. Eye Res.* **2009**, *88*, 226–234.
(2) Duncan, G.; Bushell, A. R. *Exp. Eye Res.* **1975**, *20*, 223–230.
(3) Hightower, K. R.; Farnum, R. *Exp. Eye Res.* **1985**, *41*, 565–568.
(4) David, L. L.; Shearer, T. R. *Invest. Ophthalmol. Vis. Sci.* **1984**, *25*, 1275–1283.
(5) Sanderson, J.; Marcantonio, J. M.; Duncan, G. *Invest. Ophthalmol. Vis. Sci.* **2000**, *41*, 2255–2261.
(6) Marcantonio, J. M.; Duncan, G.; Rink, H. *Exp. Eye Res.* **1986**, *42*, 617–630.
(7) Shearer, T. R.; Ma, H.; Fukiage, C.; Azuma, M. *Mol. Vis.* **1997**, *3*, 8.
(8) Sharma, Y.; Rao, C. M.; Narasu, M. L.; Rao, S. C.; Somasundaram, T.; Gopalakrishna, A.; Balasubramanian, D. *J. Biol. Chem.* **1989**, *264*, 12794–12799.
(9) Shearer, T. R.; Throneburg, D. B.; Shih, M. *Ophthalmic Res.* **1996**, *28* (Suppl 2), 109–114.
(10) Shearer, T. R.; Shih, M.; Azuma, M.; David, L. L. *Exp. Eye Res.* **1995**, *61*, 141–150.
(11) Hiraoka, T.; Clark, J. I.; Li, X. Y.; Thurston, G. M. *Exp. Eye Res.* **1996**, *62*, 11–19.
(12) Ostadalova, I.; Babicky, A.; Obenberger, J. *Experientia* **1978**, *34*, 222–223.
(13) Liao, J. H.; Chen, C. S.; Maher, T. J.; Liu, C. Y.; Lin, M. H.; Wu, T. H.; Wu, S. H. *Chem. Res. Toxicol.* **2009**, *22*(3), 518–525.

Published on Web 12/07/2010

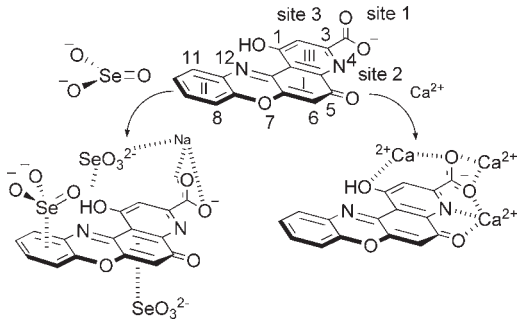

Figure 1. Ditopic complexation of PRX with selenite and calcium ions.

provided evidence that selenite enters the lens. The accumulation of selenite in lenses may cause cataract formation and may provide an explanation for the high selenium content present with increased opacification in human lenses.[16] The ability of drugs to chelate and consume the calcium and selenite ions appears to be a possible therapeutic pathway. To this end, we examined the properties of ditopic complexation for PRX and explored its mechanism of action (Figure 1).

Eye drop solution-Catalin containing claimed active component PRX (1-Hydroxy-5-oxo-5*H*-pyrido[3,2-*a*]phenoxazine-3-carboxylic acid sodium salt) introduced in 1958 and is known for its therapeutic effectiveness in suppressing the progression of senile cataracts, especially in delaying the progress of nuclear cataracts in human eyes.[17−19] The pyridophenoxazine structure resembles xanthommatin, an eye pigment of insects, which is a potent suppressor of radicals.[20] Though PRX has been applied and used clinically as an anticataract agent for many years,[21−23] there is little scientific evidence to prove its effectiveness and few investigations regarding its mechanism of action at a molecular level.[24,25] Even a report entitled "Why are physicians not persuaded by scientific evidence?" was published in 2006 to criticize doctors' prescription behaviors of PRX.[25] In view of anticataractogenesis, the ditopic complexation of calcium and selenite ions with a β-hydroxylcarboxylate unit and conjugated double bond of astaxanthin[13,26,27] seems to indicate that the polar functional groups and aromatic rings of PRX could provide the same ditopic therapy against cataractogenesis. Drugs designed with ditopic properties have been synthesized.[28−31] For example, a covalently coupled ditopic copper−platinum complex is able to recognize and cleave DNA in the major and minor grooves.[32] Another example is a combined zidovudine nucleotide and drug delivery Zn^{2+} complex that serves as a reverse transcriptase inhibitor, which may possibly offer a new cocktail for the treatment of acquired immunodeficiency syndrome.[33] In view of these applications and to investigate the therapeutic mechanisms of PRX, UV/vis, FT-IR, isothermal titration calorimetry (ITC), and ab initio calculations were utilized for monitoring PRX while it was titrated with various concentrations of selenite or calcium ions, two important factors for selenite-induced cataractogenesis.

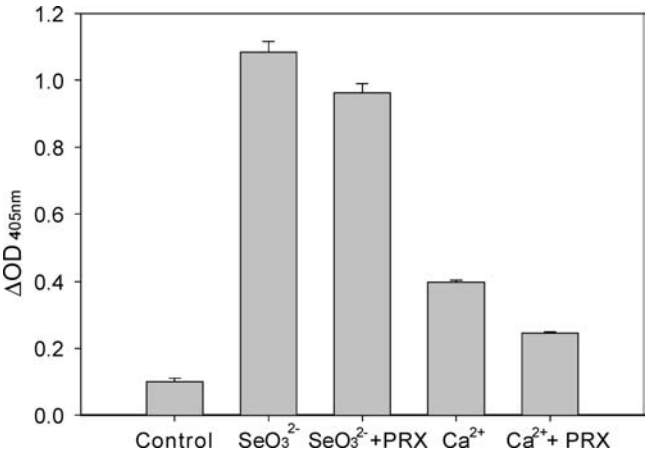

Figure 2. In vitro lens Crystallin turbidity assays. Selenite (10 mM) or calcium (10 mM) ions were applied to induce the turbidity of lens crystallins (50 mg/mL). PRX (1 μM) was shown to attenuate either selenite- or calcium-induced turbidity ($p < 0.001$). Turbidity was measured at 405 nm. Control: lens Crystallin only.

2. Results

2.1. In Vitro Lens Crystallin Turbidity Assays: Removal of Both Ca^{2+} and SeO_3^{2-} Ions by PRX. To elucidate the effects of PRX, we first used an excess of sodium selenite or calcium chloride to induce the aggregation of lens crystallins with or without the presence of PRX. As seen in Figures 2, PRX showed the ability to reduce the turbidity of lens crystallin solution, caused by selenite and calcium, by 11% and 38% ($p < 0.001$), respectively. We presumed that PRX may trap the selenite and calcium ions away from crystallin. Thus, selenite ions would likely interact with PRX first, rather than with the thiol groups of crystallins, resulting in the amelioration of selenite-induced crystallin turbidity by PRX. Because of the capability of complex formation with selenite or calcium ions, the

(14) Shearer, T. R.; Anderson, R. S.; Britton, J. L. *Curr. Eye Res.* **1982**, *2*, 561–564.
(15) Gupta, S. K.; Trivedi, D.; Srivastava, S.; Joshi, S.; Halder, N.; Verma, S. D. *Nutrition* **2003**, *19*, 794–799.
(16) Dawczynski, J.; Winnefeld, K.; Konigsdorffer, E.; Augsten, R.; Blum, M.; Strobel, J. *Klin. Monatsbl. Augenheilkd.* **2006**, *223*, 675–680.
(17) Nishizaki, K. I., K. *Folia Ophthalmol. Jpn.* **1975**, *26*, 1087–1090.
(18) Yuge, T. T., H; Ozasa, K. J. *Eye* **1988**, *5*, 1615–1618.
(19) Okamoto, T. *Folia Ophthalmol. Jpn.* **1975**, *26*, 1335–1345.
(20) Fujiwara, H.; Tanaka, N.; Suzuki, T. *Nippon Ganka Gakkai Zasshi* **1991**, *95*, 1071–1076.
(21) Kociecki, J.; Zalecki, K.; Wasiewicz-Rager, J.; Pecold, K. *Klin. Oczna* **2004**, *106*, 778–782.
(22) Chandorkar, A. G.; Albal, M. V.; Bulakh, P. M.; Jain, P. K. *Indian J. Ophthalmol.* **1978**, *26*, 6–8.
(23) Bulakh, P. M.; Chandorkar, A. G.; Balsara, J. J.; Ranade, S. M.; Albal, M. V. *Indian J. Ophthalmol.* **1980**, *28*, 1–3.
(24) Ciuffi, M.; Neri, S.; Franchi-Micheli, S.; Failli, P.; Zilletti, L.; Moncelli, M. R.; Guidelli, R. *Exp. Eye Res.* **1999**, *68*, 347–359.
(25) Sekimoto, M.; Imanaka, Y.; Kitano, N.; Ishizaki, T.; Takahashi, O. *BMC Health Serv. Res.* **2006**, *6*, 92.
(26) Chen, C. S.; Wu, S. H.; Wu, Y. Y.; Fang, J. M.; Wu, T. H. *Org. Lett.* **2007**, *9*, 2985–2988.
(27) Wu, T. H.; Liao, J. H.; Hou, W. C.; Huang, F. Y.; Maher, T. J.; Hu, C. C. *J. Agric. Food Chem.* **2006**, *54*, 2418–2423.
(28) Rosa, D. T.; Young, V. G.; Coucouvanis, D. *Inorg. Chem.* **1998**, *37*, 5042–5043.
(29) Senthilvelan, A.; Ho, I. T.; Chang, K. C.; Lee, G. H.; Liu, Y. H.; Chung, W. S. *Chemistry* **2009**, *15*, 6152–6160.
(30) Schmuck, C.; Rupprecht, D.; Junkers, M.; Schrader, T. *Chemistry* **2007**, *13*, 6864–6873.
(31) Iwamoto, S.; O., M.; Sasaki, Y.; Ikeda, A.; Kikuchi, J. I. *Tetrahedron* **2004**, *60*, 9841–9847.
(32) Hoog, P.; Boldron, C.; Gamez, P.; Sliedregt-Bol, K.; Roland, I.; Pitie, M.; Kiss, R.; Meunier, B.; Reedijk, J. *J. Med. Chem.* **2007**, *50*, 3148–3152.
(33) Aoki, S.; H., Y.; Kimura, E. *J. Am. Chem. Soc.* **1998**, *120*, 10018–10026.

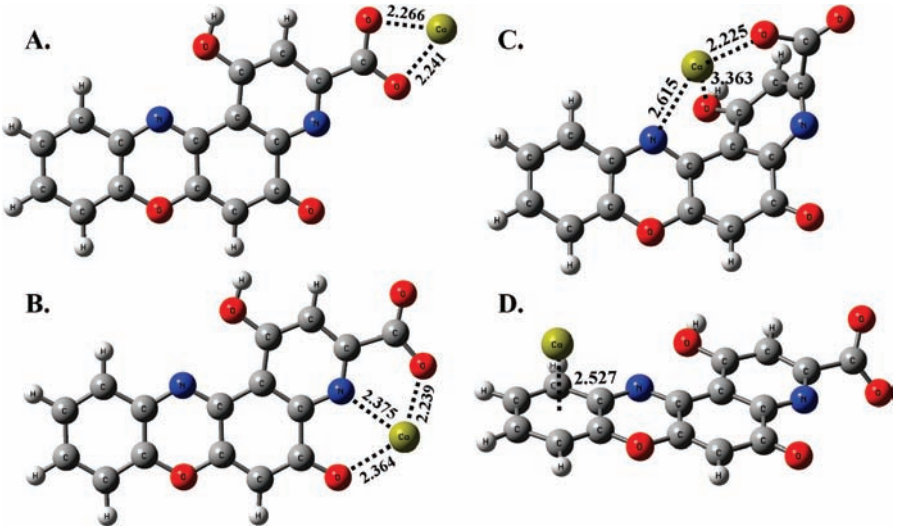

Figure 3. Four plausible structures of Ca^{2+}/PRX adducts. The stabilization energies of A−D obtained by B3LYP/6-31+G(d) are 291.74, 340.26, 258.02, and 181.41 kcal/mol, respectively. The binding capability was ranked as site 2 > site 1 > site 3 > ring II.

observed protective effects of PRX on the lens protein might have resulted from its ditopic chelating activity.

2.2. Ab initio Studies of Binding Ca^{2+} Cations and SeO_3^{2-} Anions with PRX: Preview Section. The possible sites on PRX anions available for binding Ca^{2+} or SeO_3^{2-} were first investigated by molecular orbital calculations. These theoretical results could then be employed as complementary and/or supplementary information in understanding the mechanism of the ion-binding capability exhibited by the PRX anion. These findings in return lay the foundation for future studies, such as improving the above-stated therapeutic efficiency of PRX by increasing its binding strength to SeO_3^{2-} by introducing suitable electron-withdrawing group on ring I of PRX, examining the influence of the replacement of −OH with −OR on the metal ion binding performance of the PRX anion, and avoiding the over removal of the Ca^{2+} ion by esterification (of COO^-, site 2 in Figure 1).

2.2.1. Ca^{2+}/PRX or Na^+/PRX Adducts. Having tried various input configurations subjected to B3LYP/6-31+G(d) geometry optimizations, we obtained four plausible structures as displayed in Figure 3. An analysis of stabilization energy (SE) values for the four adducts revealed that the site preference for Ca^{2+} increased in the following order: ring II < site 3 < site 1 < site 2. Similar results were found for Na^+/PRX (obtainable by B3LYP optimizations) but with smaller SE values than their Ca^{2+}/PRX analogues (see Supporting Information, Figure S1). Lewis acid−base interactions were responsible for the binding ability of PRX. These results suggest that, microscopically, one single Ca^{2+} (or Na^+) might jump among the four sites with different lifetimes. Furthermore, replacements of Na^+ in Na^+/PRX with Ca^{2+} were energetically favored. Macroscopically, Ca^{2+} cations might attack PRX^- at ring II and sites 1−3 with different probabilities or they might replace Na^+ cation(s) likely residing in ring II and sites 1−3 to form more stable complexes.

2.2.2. Binding of the SeO_3^{2-} Anion by the PRX Anion. On the basis of our previous studies,[13] the possible SeO_3^{2-} binding observed for the PRX anion in the turbidity experiments would most likely result from the numerous π-systems (rings I, II and III in Figure 1). The only possible structure of the SeO_3^{2-}/PRX adducts obtainable by B3LYP optimizations is presented in Supporting Information, Figure S2. This structure was only slightly energetically favored by H-bond formation between the two negatively charged species. The DFT/B3LYP optimizations did not support binding of the SeO_3^{2-} anion with any ring of PRX, which was mainly due to the large repulsive energies (xx, yy, zz, for rings I, II, and III, respectively) encountered by SeO_3^{2-} when fixed at the π-systems of PRX.

To evaluate the interaction of SeO_3^{2-} with the ring π-systems of PRX, we performed potential energy curve (PEC) and single-point energy (SPE) calculations by HF, DFT/B3LYP, and MP2 methods. In the first PEC calculations, we searched for the best orientation of SeO_3^{2-} and each ring by scanning dihedral angles between SeO_3^{2-} and ring II (from 0 to 120° with increments of 1° and with the distance between the Se atom and the center X being fixed at 3.2 Å). After finding the lowest-energy dihedral angle for each ring, we carried out the second part of the PEC calculations by scanning over Se—X distances (from 2.5 Å to 7.5 Å with increments of 0.1 Å) with the angle fixed at the lowest-energy orientation (see Figure 4). The latter PEC calculations were carried out by HF/6-31G, B3LPY/6-31+G(d), and MP2/6-31+G(d) methods. These procedures were then repeated for rings I and III as seen in Figure 4A−C.

The results (see Figure 4D−F) have a 3-fold significance. First, the energy well (Figure 4E) found for ring II by MP2 calculations indicated that a negative force exists between the SeO_3^{2-} anion and ring II. Additionally, this force outweighed the repulsive force of the earlier approach, as shown by the positive slopes. Second, this energy well obtained by MP2 method was evidently more obtainable than those by either DFT/B3LYP or HF calculations. This observation is consistent with the statement "MP2 calculations have been reported as a more suitable method, than either general DFT or HF, for calculating weak $\pi-\pi$ interactions".[34−41] Lastly, the $\pi-\pi$ interaction can hardly be seen even by MP2 calculations for ring III

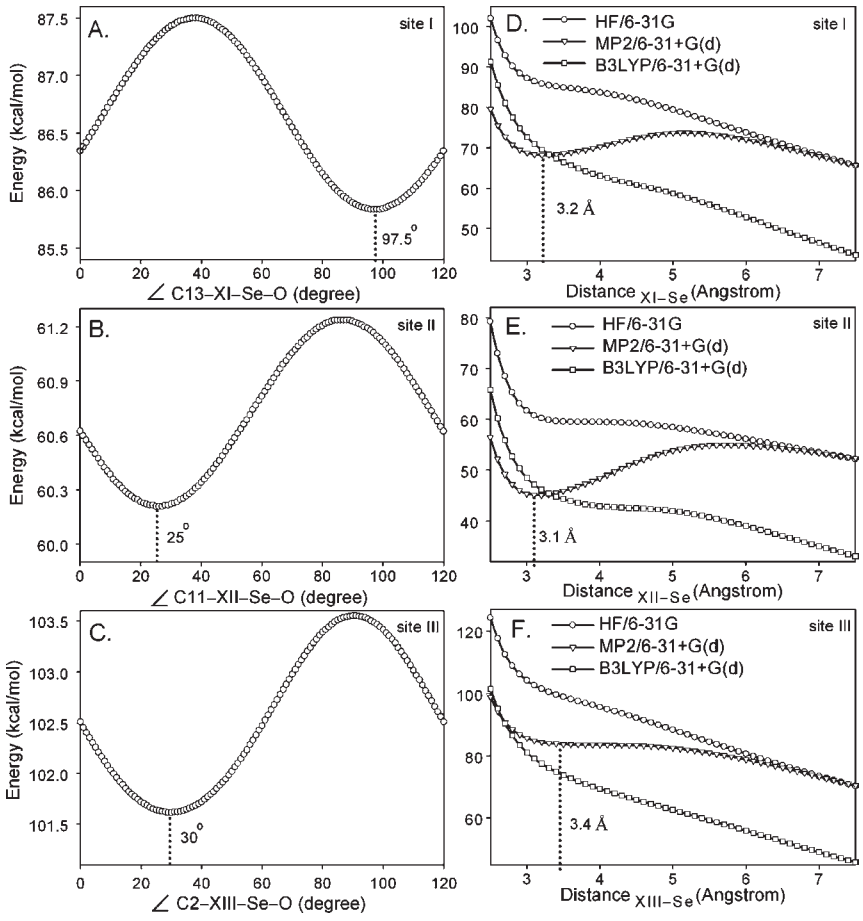

Figure 4. Potential energy curves obtained by HF/6-31G single-point energy calculations scanning over angles with a fixed Se—Xn distance of 3.2 Å for ring I (A), ring II (B) and ring III (C); potential energy curves obtained by HF/6-31G single-point energy calculations scanning over distances with fixed angles at 96° for ring I (D), at 25° for ring II (E) and at 29° for ring III (F).

(see Figure 4F). This finding allowed us to conclude that if $\pi-\pi$ interactions can somehow be found experimentally, these ring systems of PRX would show different interaction capabilities with SeO_3^{2-} (Table 1). Specifically, they would follow the trend III < I < II, which is understood based on the repulsive forces exerted by the negatively charged carboxyl group.

2.2.3. Binding of the SeO_3^{2-} Anion with Ring Systems of the PRX Anion in the Presence of Na^+. To calculate physically meaningful $\pi-\pi$ stacking energies (energy lowering and shown by positive values of SE), we performed PEC calculations on the imaging adducts of Na^+-PRX (optimized structures with Na^+ attached to site 1 or site 2) and SeO_3^{2-}. The Na^+ cations might enter sites 1, 2, and 3 through coordination of the lone-pair electrons of oxygen atoms with first priority at site 2 (SE = 151 kcal/mol), followed by site 1 (SE = 136 kcal/mol) and then site 3 (SE = 90 kcal/mol), as stated earlier (see Supporting Information, Figure S1). For either site 1 or site 2 sodium-attached PRX anion, the SeO_3^{2-} anion was then attracted to rings I, II, and III, as displayed in Figure 5.

Table 1. Stabilization Energies for Na^+-PRX/SeO_3^{2-} at Rings I to III

site	E (kcal/mol)[a]	E_{BSSE} (kcal/mol)[b]
ring I	291	286
ring II	339	336
ring III	266	258

[a] $E = E_{complex} - \sum E_{monomer}$. [b] Bitgate Server Software Environment (BSSE) was conducted by the Counterpoise (CP) method.

The energy well presented in Figure 5 revealed that the binding of SeO_3^{2-} with the ring system(s) was energetically favored and induced by Na^+ cation(s). In all of the Na^+-coordinated structures, ring III was least favored for SeO_3^{2-} binding judged by the least values of SE (see Figures 4D, 4E, and 4F). The theoretical studies presented here predict that the most likely mechanism for Na^+-PRX/SeO_3^{2-} complexation can be described by "Na^+ coordination first and followed by SeO_3^{2-}-binding". A simplified complex formation of $Na^+/Na^+/SeO_3^{2-}$ and benzene obtained by fully optimizing B3LYP/6-31+G(d) is shown in Figure 6. Lacking the coordination site for Na^+ cation(s), the sandwiched structure also provides a

(34) Jaffe, R. L.; Smith, G. D. *J. Chem. Phys.* **1996**, *105*, 2780–2788.
(35) Hobza, P.; Selzle, H. L.; Schlag, E. W. *J. Phys. Chem.* **1996**, *100*, 18790–18794.
(36) Tsuzuki, S.; Uchimaru, T.; Matsumura, K.; Mikami, M.; Tanabe, K. *Chem. Phys. Lett.* **2000**, *319*, 547–554.
(37) Sinnokrot, M. O.; Valeev, E. F.; Sherrill, C. D. *J. Am. Chem. Soc.* **2002**, *124*, 10887–10893.
(38) Sinnokrot, M. O.; Sherrill, C. D. *J. Phys. Chem. A* **2004**, *108*, 10200–10207.
(39) Sinnokrot, M. O.; Sherrill, C. D. *J. Am. Chem. Soc.* **2004**, *126*, 7690–7697.
(40) Sinnokrot, M. O.; Sherrill, C. D. *J. Phys. Chem. A* **2006**, *110*, 10656–10668.
(41) Arnstein, S. A.; Sherrill, C. D. *Phys. Chem. Chem. Phys.* **2008**, *10*, 2646–2655.

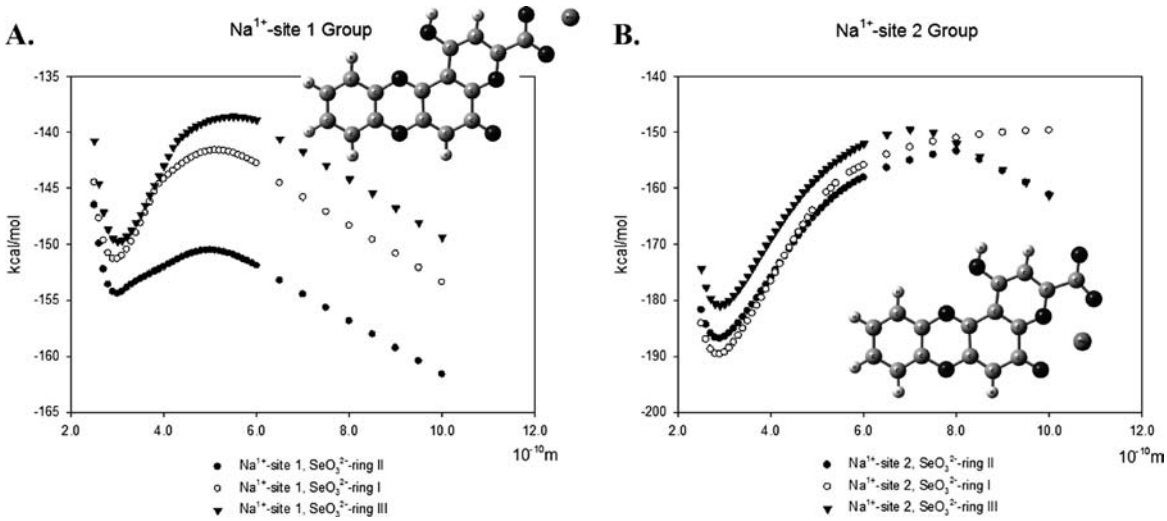

Figure 5. Potential energy/distance curves of PRX/Na^+/SeO_3^{2-} complexes for different recognition sites I−III. The scanning calculations were performed by MP2/6-31+G(d). The optimized geometry of SeO_3^{2-} and PRX/Na^+ complexes was obtained by HF/6-31G. (A) The Na^+ was localized at site 1, and the dihedral angles of relatively lower energy of PRX/SeO_3^{2-} were 32°, 90°, and 46° for sites I−III. (B) The Na^+ was localized at site 2, and the dihedral angles of relatively lower energy of PRX/SeO_3^{2-} were 33°, 2°, and 11° for sites I−III.

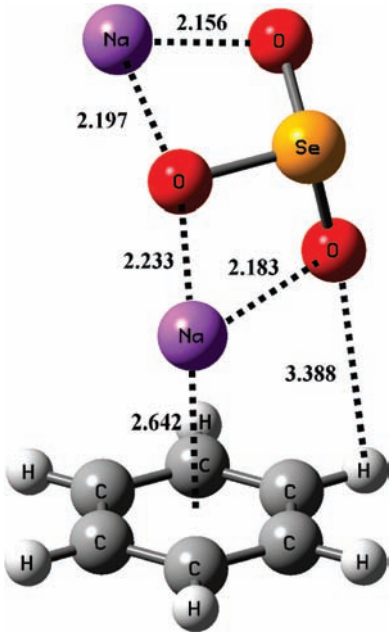

Figure 6. Optimized geometry of the benzene/Na_2SeO_3 complex was obtained by B3LYP/6-31+G(d). The sodium cation can be sandwiched by the two π-systems.

Na^+-induced complex between the phenyl system and the SeO_3^{2-} anion.

2.2.4. Other SeO_3^{2-} Binding Structures in the Presence of Na^+. On the basis of the optimized structures of Na^+-PRX presented earlier, we have further optimized the possible structures of Na^+/PRX/SeO_3^{2-} (see Figures 7A−7H) by using B3LYP/6-31+G(d) method. These structures display the possible binding of SeO_3^{2-} with the peripheral binding sites of PRX in the presence of Na^+. The optimized structures show stabilization energies (binding energy) in the order F > B > G > E > C, A, D > H. It is interesting to find that the two most stabilized structures (F and B) are hydroxyl-involved binding patterns. Furthermore, proton transfer between PRX and SeO_3^{2-} is suggested by structures (F and B), indicating H-bonding between the two anions in the presence of Na^+. The optimized most stabilized structure was the neutral adduct of $Na^+/Na^+/Na^+/PRX^-/SeO_3^{2-}$ (see Supporting Information, Figure S3) with stabilization energy of 616 kcal/mol among all possible input configurations possibly found by B3LYP/6-31+G(d) optimizations.

2.3. Spectroscopic Evidence for the Interaction of PRX with SeO_3^{2-} or Ca^{2+}. 2.3.1. UV−Vis Spectroscopy. The concentration-dependent UV/Vis absorption spectra of PRX/SeO_3^{2-} and PRX/Ca^{2+} are shown in Supporting Information, Figure S4. The maximum absorbance wavelength (λ_{max}) of PRX was 434 nm. When PRX was titrated with selenite (sodium selenite), the absorbance decreased slightly with increasing molar ratios of selenite ions, and a red shift of the maximum absorbance wavelength from 434 to 438 nm was found (Supporting Information, Figure S4A). These results indicate that the selenite ion may interact with PRX and affect its chromophores. The titration of PRX was repeated with calcium (calcium perchlorate), and the absorption peaks of PRX revealed bathochromic shifts from 434 to 452 nm with an isobathic peak appearing at 385 nm (Supporting Information, Figure S4B). The absorbance intensities of PRX decreased upon titration with Ca^{2+}.

In contrast, the absorption spectra of PRX were virtually inert upon titration with sodium perchlorate (Supporting Information, Figure S5). It is evident that the change in absorption spectra of PRX arose from the presence of either calcium or selenite, not their counterions, Na^+ or ClO_4^-. The observed red-shifts and the slightly decreased intensities of λ_{max} might result from a slight influence on the aromatic resonance system of the PRX because of the PRX/Ca^{2+} and PRX/SeO_3^{2-} complex formations. The observed changes in absorbance of PRX/Ca^{2+} were more evident than PRX/SeO_3^{2-} and might be explained by the lack of an apparent charge transfer in the PRX/SeO_3^{2-} complex.

In our previous study, we observed that selenite ions tend to bind with conjugated double bonds.[13] It is reasonable

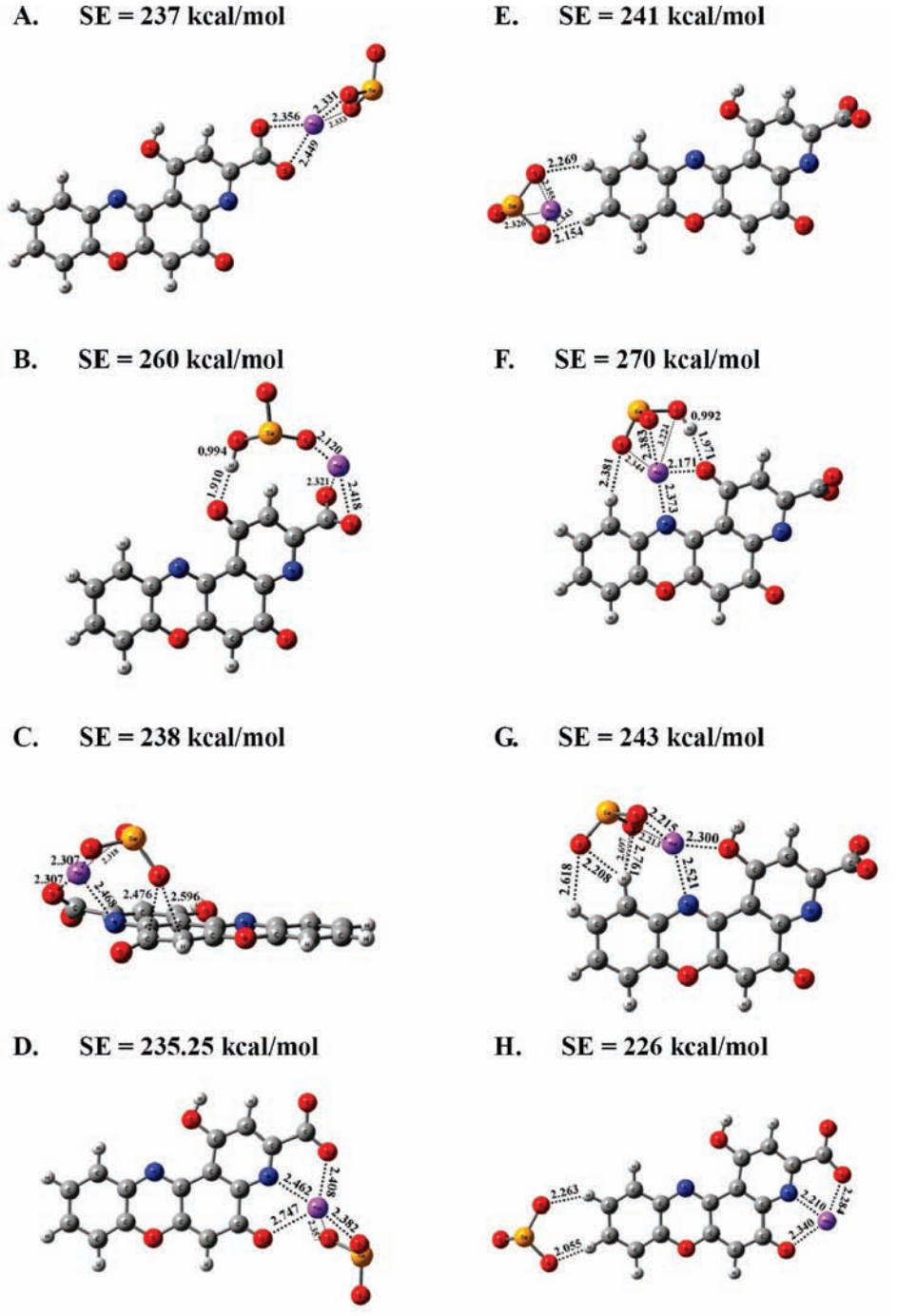

Figure 7. Possible geometries of (A−H) were optimized by using B3LYP/6-31+G(d) method.

to suggest that the binding site between the PRX/SeO_3^{2-} complex could be at the π-electron of the aromatic ring of PRX. The evenly bound selenite ions at both aromatic faces of PRX countervail the apparent charge transfer. In contrast to the PRX/SeO_3^{2-} complex, the binding of several calcium ions at different functional groups of PRX led to the apparent charge transfer while the PRX/Ca^{2+} complex formed. Additionally, no dramatic changes in UV spectra resulted from the retention of the quinone configuration of PRX during the titrations.

2.3.2. Proton NMR Spectroscopy. The proton NMR spectra shown in Figures 8 and 9 are informative concerning the PRX-SeO_3^{2-} and PRX-Ca^{2+} interactions. The introduction of SeO_3^{2-} anions by doubling its concentration sequentially (Figures 8) resulted in a concentration-dependent upfield shifts for all ring hydrogens except H2. The uniform concentration-dependent upfield shifts of the H-atoms (H8 to H11) of ring II indicate that a SeO_3^{2-} anion might approach ring II (above and/or below the ring) via $\pi-\pi$ interactions. This observation was supported by theoretical results of shielding constants calculated in our laboratories (see Supporting Information, Table S1−2). The concentration-dependent upfield shifts of H6 of ring I (Supporting Information, Table S2) shown in Figure 8 and Table 2, is also ascribed to the approach of the SeO_3^{2-} anion to ring I.

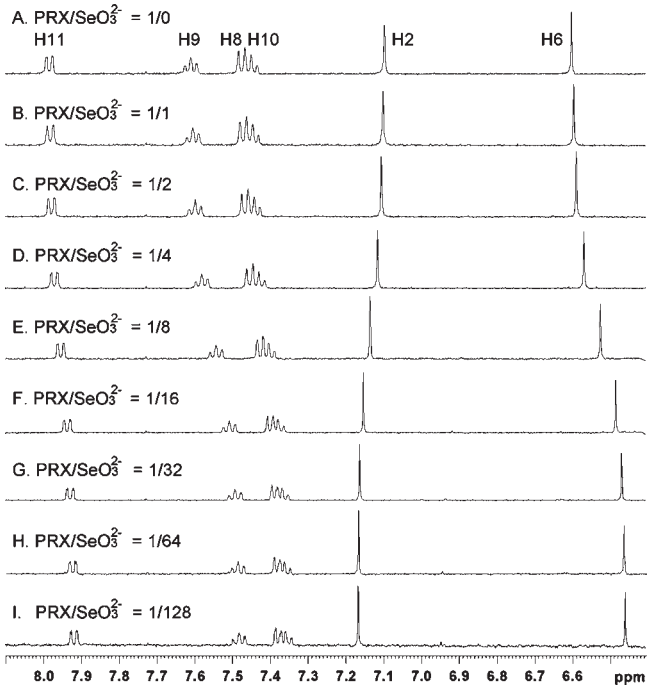

Figure 8. ^{1}H NMR spectra for PRX (0.2 mM) with various ratios of PRX/selenite in 50 mM NH_4HCO_3/d6-DMSO = 1/1, pH = 7.9.

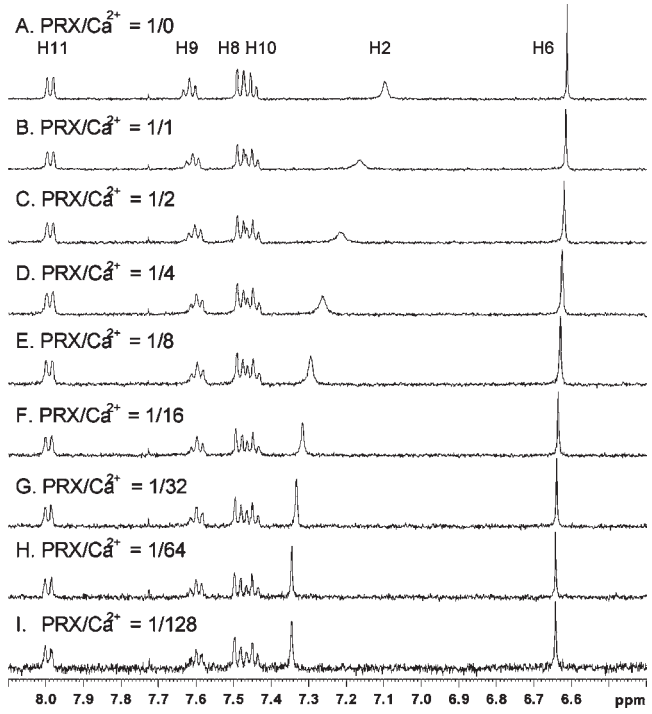

Figure 9. ^{1}H NMR spectra for PRX (0.2 mM) with various ratios of PRX/calcium in 50 mM NH_4OAc/d6-DMSO = 1/1, pH = 6.5.

More interestingly, it was found that at the first stage of SeO_3^{2-} addition (Figures 8A−8D) reveals only relatively moderate upfield response of these hydrogens. Further doubling of the SeO_3^{2-}/PRX ratio resulted in more significant upfield changes and then reached equilibrium. On the basis of the possible structures calculated for Na/PRX/SeO_3^{2-}, we propose here that the SeO_3^{2-} anions prefer the peripheral binding sites to the aromatic-planar binding sites (as demonstrated in Figures 7). Subsequent doubling the concentration of the SeO_3^{2-} forced binding to the π-ring systems (Figures 8E and 8F). This conclusion can further be drawn by the concentration-dependent shielding variations of H6 (vide infra).

Compared with ring II H-atoms, H-6 at ring I simultaneously showed upfield shifts with slightly larger extents but less sensitive responses. The latter statement was made by later reaching saturation at ring I (near the ratio PRX/SeO_3^{2-} of 1/32 in Figure 8G) than corresponding observation for ring II (near the ratio of 1/16 in Figure 8E). The values of repulsion energies between SeO_3^{2-} anion and PRX are 84 kcal/mol (ring I) and 58 kcal/mol (ring II), calculated for by HF/6-31G//MP2/6-31++G(d) after BSSE correction. These NMR spectroscopic and theoretical results suggest that PRX/SeO_3^{2-} $\pi-\pi$ interactions would also take place at ring I and must be stronger at ring I than at ring II to overcome the higher repulsion energy. We propose at the moment that the concentration-dependent ^{1}H NMR spectra can be well explained by the hybrid of the two configurations presented in Figures 5A and 5B and can be termed as "PRX/SeO_3^{2-} $\pi-\pi$ interactions induced by sodium cation(s)"

In addition to jumping among Na^+ cations to behave with lower energy, an individual SeO_3^{2-} anion in these PRX/SeO_3^{2-} solutions would migrate on two sides of the PRX plane at two possible rings to have higher freedom or larger position entropy. The reduced turbidity in Figures 2 resulting from adding PRX can be described by removal of the SeO_3^{2-} anion from aggregated SeO_3^{2-}-containing crystallins with the aid of Na^+-cations.

The opposite shifts (much less sensitive) of H2, therefore, rule out the $\pi-\pi$ interactions between SeO_3^{2-} and ring III. This observation can be explained by Coulombic repulsion: the negatively charged COO^- prevented the approach of the SeO_3^{2-} anion onto ring III. The slight deshielding of H2 can be attributed to the excess Na^+ cations added to the system along with the SeO_3^{2-} anions, which is similar to the effects of Ca^{2+} cations shielding H2 (vide infra). On the basis of the NMR data displayed in Figure 8, the SeO_3^{2-} anion reveals a dynamic behavior: it might jump between the π-systems of ring I and II.

Compared with Figure 8A, the resonance signal of H2 shown in Figure 9A was slightly more shielded and significantly broadened because of acidification (pH = 6.5). The line shape change can be explained by the lifetime broadening effects exerted by the equilibrium state, $PRX\text{-}(H) + H_2O \rightleftarrows PRX^- + H_3O^+$. The introduction of Ca^{2+} cations resulted in (1) deshielding and (2) sharpening of the H2 resonance signals. Therefore, those signals become gradually sharper because of the increasing amount of Ca^{2+} cations at site 1. Line shape analysis of H2 resonances indicated that increasing amounts of Ca^{2+} cations tended to reduce the extent of this equilibrium effect. In other words, the cation might enter site 1 in a competitive manner with the acidic proton. This argument can be further verified by the IR studies detailed below.

When more Ca^{2+} cations are present, they might have a higher tendency to enter site 3 and significantly deshield the H2 atom (charge decreasing) to reach a steady conformation in which both sites 1 and 3 are occupied by Ca^{2+} cation(s). Therefore, the sharp H2 signal becomes inert with increasing levels of Ca^{2+} cations. On the other

Table 2. Significant ^{1}H-NMR Chemical Shifts (ppm) and FT-IR Vibration Wavenumbers (cm^{-1}) for PRX, PRX/SeO_3^{2-}, and PRX/Ca^{2+} Complexes

proton	δ^HPRX	δ^HPRX/SeO_3^{2-}	$\Delta\delta^H$shift[c]	assign.[d]	δ^{IR}PRX	δ^{IR}PRX/SeO_3^{2-}
			(A) PRX/SeO_3^{2-} Complexation[a]			
H2	7.09	7.17	0.08	3COO$^-$, st	1577 (VS)	1575 (S)
H6	6.60	6.46	−0.14	4C═N, st	1560 (S)	1559 (M)
H8	7.47	7.38	−0.09	5C═O, st	1710 (S)	1676 (M)
H9	7.61	7.48	−0.13	6C═C, st	1636 (S)	1629 (VS)
H10	7.45	7.36	−0.09	12C═N, st	1716 (M)	1682 (M)
H11	7.98	7.92	−0.06	arC−C[e] st	1522 (M)	1520 (S)
			(B) PRX/Ca^{2+} Complexation[b]			
H2	7.10	7.35	0.25	3COO$^-$, st	1577 (VS)	1541 (VS), 1558 (VS)
H6	6.61	6.64	0.03	4 C═N, st	1560 (M)	1508 (M), 1521 (M)
H8	7.49	7.49	0.00	5C═O, st	1710 (S)	1683 (M), 1706 (M.)
H9	7.62	7.60	−0.02	6C═C, st	1636 (S)	1648 (M), 1652 (M)
H10	7.46	7.45	−0.01	12C═N, st	1716 (M)	1716 (M)
H11	7.99	7.99	0.00	1OH, st	−	3277 (W), 3293 (W)

[a] PRX, 0.2 mM pirenoxine in 50 mM NH_4HCO_3/d6-DMSO (1/1), pH = 7.9. PRX/SeO_3^{2-}, PRX (0.2 mM) and SeO_3^{2-} (1:128, mol/mol) for ^{1}H-NMR; PRX/SeO_3^{2-} (1:12, mol/mol) for FT-IR. [b] PRX, 0.2 mM pirenoxine in 50 mM NH_4OAc/d6-DMSO (1/1), pH = 6.5. PRX/Ca^{2+}, PRX (0.2 mM) and Ca^{2+} (1:128, mol/mol) for ^{1}H-NMR; PRX/Ca^{2+} (1:6, mol/mol) for FT-IR. [c] $\Delta\delta^H$shift = δ^HPRX/ion − δ^HPRX. [d] VS, very strong; S, strong; M, medium; W, weak. [e] The arC−C group was assigned to the alkanyl groups of the 4-hydroxylpyridine III.

hand, the resonance position signals of the other hydrogens remain virtually unchanged toward the concentration of Ca^{2+} cations. These observations rule out the interaction between Ca^{2+} cations with any ring systems of PRX. The possible sites available for PRX to bind Ca^{2+} cation(s) have been studied by B3LYP/6-31+G(d) level calculations, which yielded binding energies of 292, 340, and 258 kcal/mol for three binding sites, respectively (see also Figure 4D−F). The magnitudes of SE are consistent with the relative strengths: site II > site I > site III. The strongest PRX coordination to Ca^{2+} cations at site 2 cannot be detected by ^{1}H NMR because there are no available H atoms to serve as indices. Therefore, IR spectroscopy was performed to obtain a better understanding of the interactions of PRX with both ions (vide infra).

Similar to the effects of the Ca^{2+} cation, the downfield movements of H2 as shown in Figure 8A−G are a result of increasing amounts of sodium cations (added along with SeO_3^{2-} anions) at site 3. The relative effects of Na^+ and Ca^{2+} cations on H2 resonances were evident through their charges and could be supported by the B3LYP/6-31+G(d) results of shielding constants. Both cations have the potential to deshield H2 as illustrated in the Supporting Information, Table S3. We then searched for possible conformations of the PRX/SeO_3^{2-} adducts in the presence of sodium(s) and located Na^+ cations at sites 1 and 2. The calculated results are presented in Figure 5 and suggest that these systems are energetically favored. It is noteworthy that, for the benzene/SeO_3^{2-} adduct in the presence of Na^+ cations (Figure 6), the sodium cation can be sandwiched by the two π systems. In this circumstance, SeO_3^{2-} anions can be trapped by compounds with a benzene moiety (Figure 6).

2.3.3. IR Spectroscopy. The binding properties of PRX with selenite and calcium ions were further examined by NMR and FT-IR experiments (Table 2 and Figures 8, 9 and Supporting Information, Figure S6). In the IR data obtained for PRX/SeO_3^{2-} mixtures (1/12, Table 2A), the most significant changes were observed and assigned to 4-iminobenzoquinone I. The PRX/SeO_3^2 complexation-induced changes for 5-carbonyl (1710 cm^{-1}), 6-alkenyl (1636 cm^{-1}), and 12-imine (1716 cm^{-1}) groups were −25, −7, and −34 cm^{-1}, respectively. Additionally, the intensity for the 6-alkenyl group at 1629 cm^{-1} changed from the strong to very strong range, and the aromatic alkanyl groups at 1520 cm^{-1} of the 1-hydroxylpyridine group III changed from the medium to strong range. These results indicate that the 4-iminobenzoquinone I of PRX might play an important role in the binding of selenite ions. The decreasing intensity of the 3-carboxylate (1575 cm^{-1}) and the 4-imine (1559 cm^{-1}) groups also indicate that 4-hydroxylpyridine III could provide another binding site for selenite. The observation of upfield shifts of the aromatic protons from H6 to H11 in the ^{1}H NMR spectra suggests that the benzene ring II might also be involved in the binding of selenite ions. These results strongly indicate that PRX utilizes π-electron-rich aromatic moieties to interact with SeO_3^{2-}, which results in the change of stretching wavenumbers.

From the IR spectra of the PRX/Ca^{2+} (1/6, mol/mol) complex given in Table 2B, the functional groups of PRX were split and shifted by the addition of calcium ions. In contrast, the changes of the proton nucleus from H6 to the H11 nucleus of the PRX/Ca^{2+} complex were relatively smaller than PRX/SeO_3^{2-} complex in the ^{1}H NMR. Unlike the ligation of the π-electron of PRX with the SeO_3^{2-} anion, the polar groups of an organic molecule can provide their selective chelating ability for metal ions. With polar functional groups, sites 1−3 were primarily considered to have a calcium chelating property and were examined by FT-IR spectroscopy. Upon chelating a calcium ion in site 1, the vibration frequency of the 2-carboxylate group was split into two different wavenumbers (1541 and 1558 cm^{-1}) in the FT-IR spectra. Following calcium ion chelating at site 2, the absorption bands of the 4-imine (1508, 1521 cm^{-1}) and 5-carbonyl (1683, 1706 cm^{-1}) groups were also split into two doublet pairs. In addition to site 1 and site 2, chelating a calcium ion in site 3 also led to the split of vibration frequencies of 1-hydroxyl (3277, 3293 cm^{-1}) groups, and a downfield shift (0.25 ppm) of H2 was observed in the ^{1}H NMR spectra. These results strongly indicated that the calcium ions could be

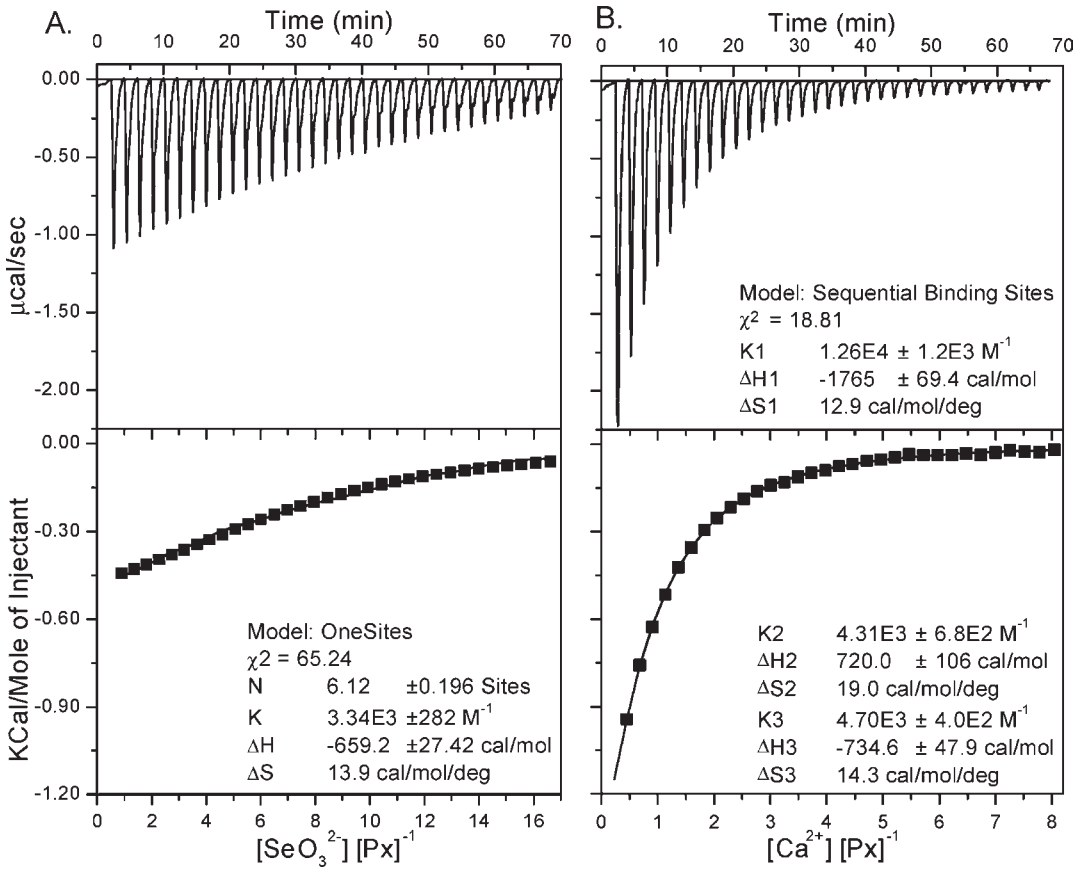

Figure 10. Binding isotherms for PRX titrated with selenite and calcium ions. Titrations of (A) 0.1 mM PRX with 8 mM Na_2SeO_3 in 50 mM NH_4HCO_3/DMSO (1:1, v/v, pH 7.9) and (B) 0.2 mM PRX with 8 mM $Ca(ClO_4)_2$ in 50 mM NH_4OAc/DMSO (1:1, v/v, pH 6.5) at 25 °C were performed using an ITC microcalorimeter. For each titration, raw data were obtained from 33 automatic injections (8 μL/injection). The integrated fitted curves show the experimental points with a one-site function for PRX/SeO_3^{2-} complex formation (A) and a sequential binding site function for PRX/Ca^{2+} complex formation (B) with the parameter $n = 3$.

coordinated by atoms (of β-ketoimine, hydroxyl, and carboxylate groups) carrying lone electron pairs with various capabilities. After chelating several calcium ions, the resonance properties of PRX might be influenced. The 6-alkene (1636 cm^{-1}) was observed to split with a red-shift (12, 16 cm^{-1}). Among those possible calcium-chelating sites, the FT-IR band shifts at site 2 were larger than those of the other two functional groups. Therefore, we speculated that site 2 might have had a better calcium binding affinity. The Ca^{2+}/PRX adducts at sites 1−3 (Figure 1) were also investigated (see Figure 3D−F). The binding energies calculated by B3LYP/6-31+G(d) at sites 1−3 were 292, 340, and 258 kcal/mol, respectively. We also obtained the binding energies by MP2/6-31++G(d,p) with BSSE correction (see Table 1). Therefore, the same conclusion for the site preference of Ca^{2+} chelation presented earlier was also predicted by our calculations.

2.4. Thermodynamic Statistics of the PRX/SeO_3^{2-} and PRX/Ca^{2+} Complexes. The binding thermodynamics of the PRX/SeO_3^{2-} and PRX/Ca^{2+} complexes were measured by ITC-titration (Figure 10, Table 3). The results clearly demonstrated that PRX was capable of binding selenite or calcium ions. Both PRX/SeO_3^{2-} and PRX/Ca^{2+} complexes yielded exothermic titration curves. Larger values of ΔS were observed and indicated that the complexes of PRX/SeO_3^{2-} and PRX/Ca^{2+} were spontaneous. The titration isotherm curve of PRX/SeO_3^{2-} was fitted with a one-site model and provided thermodynamic parameters ($\Delta H = -659.2$ cal mol^{-1} and $\Delta S = 13.9$ cal mol^{-1} K^{-1}) with stoichiometry $n = 6$. This is because there are three rings in PRX resulting in six π-conjugation faces with which to bind SeO_3^{2-} through $\pi-\pi$ stacking and also other bindings through hydrogen bonding and the sodium stabilization effect; therefore, PRX might bind at most six selenite ions. According to the FT-IR spectra of the PRX/SeO_3^{2-} complex, the aromatic 4-iminobenzoquinone I was recognized as the first critical binding ring based on the significant changes in absorption intensities. To confirm this observation, benzoquinone and hydroquinone were titrated with selenite and showed positive results (Figure 11, Supporting Information, Figure S7 and Table 3D−E). Benzoquinone ($\Delta S = 20.3$ cal mol^{-1} K^{-1}) was found to have a better affinity and higher entropy loss than hydroquinone ($\Delta S = 5.93$ cal mol^{-1} K^{-1}) when forming a complex with selenite. The entropy-driving force of selenite binding may be due to loss of water, a solvent molecule, or a counterion from the PRX/SeO_3^{2-} ligand.

The complex between PRX with calcium ions was considered to have three binding sites based on the significant changes and split doublets in the FT-IR experiment. A sequential binding model with three binding sites was applied to the ITC data analysis and fitting. The largest band shifts of the 4-imine group indicated that site 2 of PRX provided imperative binding and was recognized as the first calcium-chelating packet. The calcium binding site 2 was estimated to be the most exothermic and was

Table 3. Thermodynamic Parameters of PRX/SeO_3^{2-}, PRX/Ca^{2+}, Benzoquinone/SeO_3^{2-}, and Hydroquinone/SeO_3^{2-} Complexation at 25 °C

n	K (M^{-1})	ΔG (kcal/mol)[a]	ΔH (cal/mol)	ΔS (cal/mol)
	(A) $[SeO_3^{2-}][PRX]^{-1}$, One-Site Binding Model			
6	$(3.34 \pm 0.28) \times 10^3$	−4.81	-659.2 ± 27.42	13.9
	(B) $[SeO_3^{2-}][PRX]^{-1}2^{-1}$, Sequential Fitting Model with the Parameter $n = 3$			
1	$(6.82 \pm 1.70) \times 10^3$	−5.24	$(-2.11 \pm 0.31) \times 10^3$	10.5
2	$(1.22 \pm 0.28) \times 10^3$	−4.20	$(-3.49 \pm 1.17) \times 10^3$	2.4
3	$(3.43 \pm 0.67) \times 10^4$	−6.17	$(3.07 \pm 0.99) \times 10^3$	31.0
	(C) $[Ca^{2+}]^{-1}$ [PRX], Sequential Fitting Model with the Parameter $n = 3$			
1	$(1.26 \pm 0.12) \times 10^4$	−5.59	-1765 ± 69	12.9
2	$(4.31 \pm 0.68) \times 10^3$	−4.95	720 ± 106	19.0
3	$(4.72 \pm 0.40) \times 10^3$	−5.01	-735 ± 48	14.3
	(D) $[SeO_3^{2-}]$ [Benzoquinone]$^{-1}$, One-Site Binding Model			
2	$(5.01 \pm 0.55) \times 10^4$	−6.41	-346.4 ± 5.1	20.3
	(E) $[SeO_3^{2-}]$ [Hydroquinone]$^{-1}$, One-Site Binding Model			
2	$(7.58 \pm 0.34) \times 10^2$	−3.92	-2160 ± 106	5.9

[a] $\Delta G = -RT \ln K$.

accompanied by the highest negative Gibb's free energy ($\Delta H = -1.76$ and $\Delta G = -5.59$ kcal mol^{-1}) as presented in Table 2C. After curve fitting, positive values of enthalpy and entropy ($\Delta H = 720$ cal mol^{-1} and $\Delta S = 19.0$ cal mol^{-1} K^{-1}) were obtained for the second calcium binding site of PRX. Such unfavorable enthalpy and interaction entropy were seen in the titration of acetic acid with calcium ions and were likely due to the displacement of highly disordered water or solvent near ionic species.[42] Thus, the ITC fitting results suggest that site 1, which carried the carboxylate group, was the second calcium binding site. Another binding packet was site 3, which yielded a minor enthalpy release and a negative Gibb's free energy based on the ITC analysis of the complex ($\Delta G = -5.01$ and $\Delta H = -0.74$ UV/Vis kcal mol^{-1}). From the calculated negative Gibb's free energy (< 4.9 kcal mol^{-1}) of all these sequential calcium complexes, we concluded that the PRX/Ca^{2+} complex formation resulted from entropic effects and proceeded spontaneously. It should be noted that the binding of selenite or calcium ions to PRX was so specific that selenate (SeO_4^{2-}) or magnesium ions (Mg^{2+}) would not bind to PRX (Supporting Information, Figures S7−S8).

3. Discussion

A sequential binding model is usually applied to fit a binding isotherm for a molecule with several binding packets with the first binding site possessing the highest binding affinity. The ITC fitting functions provided by the Microcal Origin fitting software can be applied to calculate the binding isotherm for a 1:3 ratio of the PRX/SeO_3^{2-} complex at intrinsic binding sites, but not for a 1:6 ratio. Because each π-conjugation face might be able to provide almost identical binding affinity with the selenite ion, a modified fitting method was applied. By changing the molar ratio from $[SeO_3^{2-}]$/[PRX] to $[SeO_3^{2-}]$/2[PRX], the sequential fitting functions of the three binding sites were applied to fit the three pairs of statistical thermodynamic isotherms (Table 3B).

According to the FT-IR spectra of the PRX/SeO_3^{2-} complex, the aromatic 4-iminobenzoquinone I was recognized as the first critical binding ring because of the significant changes in absorption intensities with binding parameters $\Delta H = -2.11$ kcal/mol and $\Delta S = 10.5$ cal mol^{-1} K^{-1}. The value of the SeO_3^{2-}/hydroquinone complex was much weaker than that of the SeO_3^{2-}/benzoquinone complex. This tendency suggested that the benzene II of PRX was the second selenite binding group based on the smaller entropy value, $\Delta S = 2.4$ cal mol^{-1} K^{-1}. The resulting 4-hydroxylpyridine III with a carboxylate group was considered the third selenite binding group. With a negative carboxylate group at aromatic resonance III, the SeO_3^{2-}/PRX complex might cause Coulombic repulsion, which counteracted the incoming SeO_3^{2-} ions and resulted in increased enthalpy and entropy ($\Delta H = 3.07$ kcal/mol and $T\Delta S = 9.24$ kcal mol^{-1}). Obviously, a larger entropy value of 31 cal mol^{-1} K^{-1} promoted complex formation with the third selenite. The third selenite complex with aromatic ring III may not only affect the hydration or solvation of the carboxylate group, but it may also disturb the solvated molecules near the selenite ions complexed at the benzoquinone ring II. However, our data show that the third binding parameter of the PRX/SeO_3^{2-} complex was larger than the first, and it was concluded that the fused π-conjugation resonance system of the two aromatic rings II and III was involved in the phenomenon. Our reported thermodynamic parameters did not perfectly match the exact values and probably resulted from the procedure of replacing the molar ratio of $[SeO_3^{2-}]$/[PRX] with $[SeO_3^{2-}]$/2[PRX]. The reported thermodynamic data for the PRX/SeO_3^{2-} complex formation could be larger than the true values, but the change tendency should be directly proportional to the exact ones. Before a suitable fitting function can be developed to solve the multiple binding sites, our results and procedures could offer a compromise answer.

To further confirm these weak interactions, theoretical calculations of the PRX/SeO_3^{2-} complexes were performed. The results obtained by MP2/6-31+G(d) molecular orbital calculations provided theoretical evidence in support of the $\pi-\pi$ interactions between selenite and the PRX aromatic

(42) Christensen, T.; Gooden, D. M.; Kung, J. E.; Toone, E. J. *J. Am. Chem. Soc.* **2003**, *125*, 7357–7366.

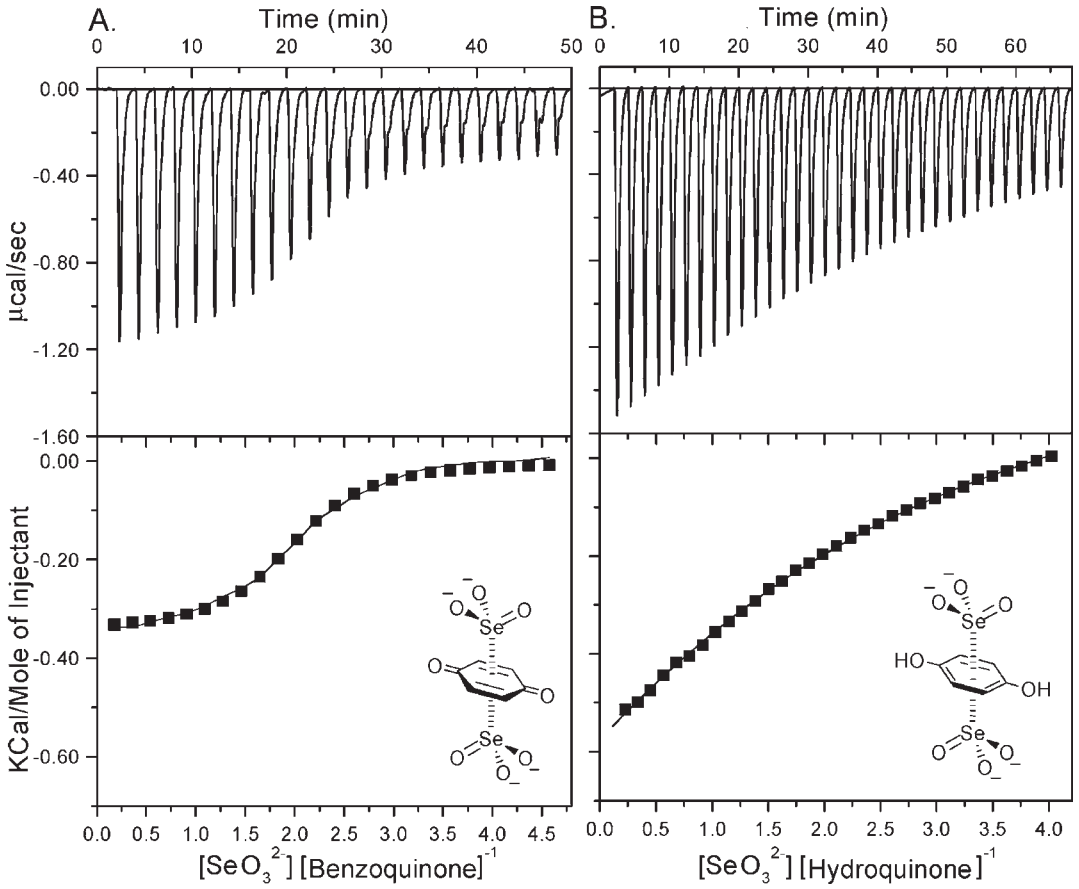

Figure 11. Binding isotherms for benzoquinone and hydroquinone titrated with selenite. Titrations of 0.2 mM (A) benzoquinone and (B) hydroquinone with 8 mM Na_2SeO_3 in 50 mM NH_4HCO_3/DMSO (1:1, v/v, pH 7.9) at 25 °C.

framework with binding energies in favor of benzoquinone, followed by the other two rings. It has been reported that the $\pi-\pi$ interactions were only suitable for MP2 or higher level theory calculations.[34−41] The energy-distance diagrams obtained by HF,[43,44] DFT/B3LYP,[45] and MP2 calculations for each possible selenite-aromatic ring center are summarized in Figure 4. The energy well can only be found in the MP2 results. This result provides evidence in support of the suggested $\pi-\pi$ interactions for the PRX/SeO_3^{2-} complex. According to current ITC data, the association constant was 3.34×10^3, which indicates that the complex between PRX and selenite was weak. Moreover, the energy minimum found in benzoquinone/selenite (ring I in Figure 3) stacking at 3.1 Å was 23 kcal/mol lower than the ring-II/selenite analogue (at a longer distance of 3.2 Å). The weakest interaction was the complex with ring III in which the energy well was not evident. The trend of stacking preference at different rings was corroborated by spectroscopic data. In the presence of sodium cations, selenite can also be trapped by the PRX/Na^+ complex (Figure 6).

All of these models suggest that selenite can bind to PRX. An earlier study showed that selenium binds to the lipids of marine algae,[46] and it was thought to bind to the π-bonding system of lipids, such as carotenoid pigments, rather than be metabolically incorporated. Our previous study also indicated that selenite binds to the electron-rich π-conjugated moiety of astaxanthin.[13] The current study also suggested that selenite would bind to the aromatic resonance moiety of various compounds with an affinity similar to astaxanthin. Therefore, we concluded that selenite will bind with compounds carrying an electron-rich π-conjugated system.

Cataracts constitute a multifactorial disease process associated with many risk factors. Although the exact causes of cataracts remain vague, protein aggregation and osmotic damage leading to a loss of transparency appear to be the main contributors to this disease.[47] Changes in hydration or electrolyte content can also lead to protein aggregation. Additionally, chemical modifications or oxidations of lens proteins may contribute to the emergence of opacities. The loss of crystalline organization causes an increase in light scattering and nuclear sclerosis in lenses. Both selenite and calcium ions could cause precipitation of lens crystallins.[13,27] Here (Figure 12), PRX was found to possess ditopic recognition properties, which provides a clinical rationale for the application of PRX for cataract prevention or therapy.

4. Experimental Section

General Information. PRX sodium was purchased from Hangzhou Dayangchem Co., Ltd. (China). Sodium selenite (Na_2SeO_3), sodium selenate (Na_2SeO_4), sodium sulfite (Na_2SO_3), sodium sulfate (Na_2SO_4), calcium perchlorate [$Ca(ClO_4)_2$], and magnesium perchlorate [$Mg(ClO_4)_2$] were purchased from

(43) Roothaan, C. C. J. *Rev. Mod. Phys.* **1960**, *32*, 179–185.
(44) Binkley, J. S.; Pople, J. A.; Dobosh, P. A. *Mol. Phys.* **1974**, *28*, 1423–1429.
(45) Becke, A. D. *J. Chem. Phys.* **1993**, *98*, 5648–5652.
(46) Gennity, J. M.; Bottino, N. R.; Zingaro, R. A.; Wheeler, A. E.; Irgolic, K. J. *Biochem. Biophys. Res. Commun.* **1984**, *118*, 176–182.
(47) Bunce, G. E.; Kinoshita, J.; Horwitz, J. *Annu. Rev. Nutr.* **1990**, *10*, 233–254.

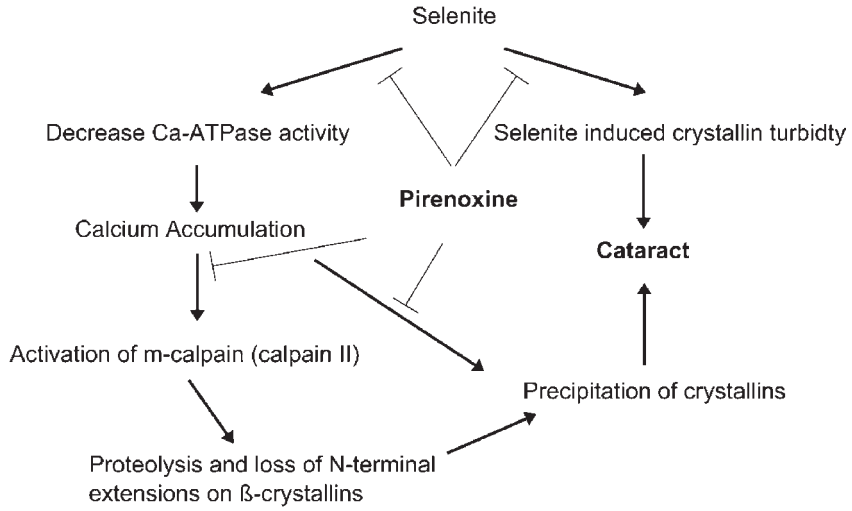

Figure 12. Proposed mechanism of selenite nuclear formation and the effects of PRX. Selenite induces precipitation of crystallins and leads to decreased Ca^{2+}-ATPase activity. The decrease of Ca^{2+}-ATPase activity causes calcium accumulation and activation of *m*-calpain. Both calcium ions and calpain cause the precipitation of crystallins. The ditopic recognition properties of pirenoxine provide a rationale for using pirenoxine as an agent to prevent cataract formation.

Sigma-Aldrich Chemical Co. (St. Louis, MO., U.S.A.); HPLC-grade dimethyl sulfoxide (DMSO) was purchased from Merck Chemical Co. (Darmstadt, Germany).

In Vitro Lens Crystallin Turbidity Assays. Porcine lenses were decapsulated and homogenized in buffer containing 50 mM Tris-HCl, 0.1 M NaCl, 5 mM EDTA, 0.01% β-mercaptoethanol, and 0.02% sodium azide, pH 8.0. After centrifugation at 16060 g for 30 min, the supernatant was collected, and the protein concentration was determined according to the Bradford method (BioRad Laboratories, U.S.A.). The Crystallin turbidity assays of PRX involved two in vitro anti-cataract screening systems, which used excess calcium or sodium selenite to induce lens protein turbidity. Lens protein with buffer only was used as a control. Crystallins with calcium ($CaCl_2$, 10 mM) or selenite (Na_2SeO_3, 10 mM) ions were also used as controls. Buffers with or without PRX were used as blanks. Samples were incubated at 37 °C for 5 days. The turbidity was measured at 405 nm using a UV/vis spectrophotometer.

Methods of Calculations. Ab initio studies of the ditopic property of PRX (or Na^+-PRX) on Ca^{2+} and SeO_3^{2-} were performed at different levels of calculations. Geometric optimizations were carried out using the hybrid density functional theory adopting the Becke three-parametrized correlation functional[48] and the Lee−Yang−Parr exchange correlation functional (DFT/B3LYP). These calculations included HF, MP2[48]/6-31+G(d),[49−54] and/or DFT/B3LYP using 6-31+G(d) basis molecular orbital calculations, employing the Gaussian 03 package[55] (RevB-02 NBO version 3−1) for PRX/SeO_3^{2-} and PRX/Ca^{2+} complexes. Schematic representations of optimized geometries for PRX/SeO_3^{2-} and PRX/Ca^{2+} are shown in Figure 3. The binding energies of PRX/SeO_3^{2-} and PRX/Ca^{2+} adducts were studied by MP2[48]/6-31+G(d)[49−54] and B3LYP/6-31+G(d) molecular orbital calculations employing the Gaussian 03 package (RevB-02 NBO version 3−1).[55] After the lowest-energy orientation of the PRX/SeO_3^{2-} adduct was found (Figure 3A−C), single-point calculations were performed at various distance-(between Se atoms and the center of the ring) angle curves of different PRX/SeO_3^{2-} complexes at the MP2/6-31+G(d) level (Figure 4A−C). These results show relatively lower energies at 97.5°, 25°, and 30° for sites I−III, respectively.

NMR Spectra. NMR experiments were performed on a Bruker Avance NMR spectrometer (400 and 500 MHz) at 300 K. Chemical shifts of ^{1}H NMR spectra were reported relative to DMSO (δH, 2.50 ppm).

UV/vis Titration Studies of PRX/Ca^{2+}, PRX/Mg^{2+}, PRX/SeO_3^{2-}, PRX/SeO_4^{2-}, PRX/SO_3^{2-}, and PRX/SO_4^{2-} Complexes. To prevent the precipitation of calcium phosphate or calcium carbonate in sodium phosphate or ammonium carbonate buffer solutions, ammonium acetate (50 mM NH_4OAc, pH = 6.5) was chosen as the buffer solution for PRX/ion complexes. A working solution of 50 μM PRX was prepared in 50 mM NH_4OAc, and a 1-mL aliquot was transferred to a 1-cm cuvette. The ionic salt (25 mM) and PRX (50 μM) were mixed as an ion-source stock solution in the same buffer solution to prevent the dilution of PRX during the titration. The absorbances of PRX at various ratios of PRX/ions (1:0 to 1:128) were then determined with a Hitachi U-3300 spectrophotometer (Tokyo, Japan).

Isothermal Titration Calorimetry of PRX/SeO_3^{2-}, PRX/SeO_4^{2-}, PRX/SO_3^{2-}, and PRX/SO_4^{2-} Mixtures. The heat produced by the complex formation between 0.1 mM PRX (1.436 mL in 50 mM NH_4HCO_3, DMSO = 1/1, pH = 7.9) and 8 mM Na_2SeO_3, Na_2SeO_4, Na_2SO_3, or Na_2SO_4 (300 μL in the same mixing buffer, pH = 7.4) at 25 °C with continuous stirring (300 rpm) was analyzed using Origin software. The integration

(48) Moller, C.; Plesset, M. S. *Phys. Rev.* **1934**, *46*, 0618–0622.
(49) Rassolov, V. A.; Pople, J. A.; Ratner, M. A.; Windus, T. L. *J. Chem. Phys.* **1998**, *109*, 1223–1229.
(50) Pople, P. C. H. a. J. A. *Theoret. Chim. Acta* (*Berl.*) **1973**, *28*, 213–222.
(51) Clark, T.; Chandrasekhar, J.; Spitznagel, G. W.; Schleyer, P. V. *J. Comput. Chem.* **1983**, *4*, 294–301.
(52) Frisch, M. J.; Pople, J. A.; Binkley, J. S. *J. Chem. Phys.* **1984**, *80*, 3265–3269.
(53) Latajka, Z.; Scheiner, S. *Chem. Phys. Lett.* **1984**, *105*, 435–439.
(54) Hehre, W. J.; Ditchfield, R.; Pople, J. A. *J. Chem. Phys.* **1972**, *56*, 2257.
(55) Frisch, M. J., Trucks, G. W., Schlegel, H. B., Scuseria, G. E., Robb, M. A., Cheeseman, J. R., Montgomery, J. A., Vreven, Jr., T., Kudin, K. N., Burant, J. C., Millam, J. M., Iyengar, S. S., Tomasi, J., Barone, V., Mennucci, B., Cossi, M., Scalmani, G., Rega, N., Petersson, G. A., Nakatsuji, H., Hada, M., Ehara, M., Toyota, K., Fukuda, R., Hasegawa, J., Ishida, M., Nakajima, T., Honda, Y., Kitao, O., Nakai, H., Klene, M., Li, X., Knox, J. E., Hratchian, H. P., Cross, J. B., Adamo, C., Jaramillo, J., Gomperts, R., Stratmann, R. E., Yazyev, O., Austin, A. J., Cammi, R., Pomelli, C., Ochterski, J. W., Ayala, P. Y., Morokuma, K., Voth, G. A., Salvador, P., Dannenberg, J. J., Zakrzewski, V. G., Dapprich, S., Daniels, A. D., Strain, M. C., Farkas, O., Malick, D. K., Rabuck, A. D., Raghavachari, K., Foresman, J. B., Ortiz, J. V., Cui, Q., Baboul, A,. G., Clifford, S., Cioslowski, J., Stefanov, B. B., Liu, G., Liashenko, A., Piskorz, P., Komaromi, I., Martin, R. L., Fox, D. J., Keith, T., Al-Laham, M. A., Peng, C. Y., Nanayakkara, A., Challacombe, M., Gill, P. M. W., Johnson, B., Chen, W., Wong, M. W., Gonzalez, C., Pople, J. A. *Gaussian 03*, revision B.02; Gaussian, Inc.: Pittsburgh, PA, 2003.

of the heat pulses obtained from each titration was fitted to a sequential binding curve.

Isothermal Titration Calorimetry of PRX/Ca^{2+} and PRX/Mg^{2+} Mixtures. ITC measurements were conducted on a VP-ITC Microcalorimeter (Microcal Inc., Northampton, U.S.A.). The heat produced by the complex formation while 0.2 mM PRX (1.436 mL in 50 mM NH_4OAc/DMSO = 1/1, pH = 6.5) was mixed with 8 mM calcium perchlorate or magnesium perchlorate (300 μL in the same mixing solvent) at 25 °C with continuous stirring (300 rpm) was analyzed using Origin software (Edition 7.0, Microcal Inc.). The integration of the heat pulses obtained from each titration was fitted to a sequential binding curve to obtain the enthalpy change (ΔH in cal/mol), the entropy change (ΔS in cal mol^{-1} K^{-1}), the association constant (K_{assoc} in M^{2-}), and the number of binding sites (n, per compound).

FT-IR Spectroscopy of PRX/Ca^{2+} and PRX/SeO_3^{2-} Mixtures. The absorbances of PRX, PRX/Ca^{2+} (1/3 and 1/6), and PRX/SeO_3^{2-} (1/6 and 1/12) were determined with a Bruker Tensor 27 spectrophotometer (Ettlingen, Germany) with a solid state MIRacleTM single-reflection horizontal ATR (PIKE Tech. Inc., Madison, U.S.A.). For PRX/Ca^{2+} preparation, a 1 mM PRX (8 mL in 50 mM NH_4OAc) solution was mixed with various ratios of a calcium ion stock solution (1 M). For PRX/SeO_3^{2-} preparation, a 1 mM PRX (8 mL in 50 mM NH_4HCO_3) solution was mixed with various ratios of a selenite ion stock solution (1 M). The mixtures were freeze-dried with a spinning vacuum to yield lead black solids.

Acknowledgment. We greatly appreciate Dr. Shu-Chuan Jao (Biophysics Core Facility, Academia Sinica) for her technical support in ITC and NMR. This study was supported by grants from the National Science Council (NSC 98-2313-B-038-002-MY3), Shin Kong Wu Ho-Su Memorial Hospital (SKH-TMU-96-14), and Academia Sinica, Taiwan.

Supporting Information Available: Further details are given in Tables S1−S3 and Figures S1−S9. This material is available free of charge via the Internet at http://pubs.acs.org.